Impact of Fast Frequency Response on Power System Transient Stability

IMPACT OF FAST FREQUENCY RESPONSE ON POWER SYSTEM TRANSIENT STABILITY

Zaichun Zhang[1], Surat Asvapoositkul[1], Robin Preece[1*]

[1]Department of Electrical and Electronic Engineering, The University of Manchester, Manchester, UK
**robin.preece@manchester.ac.uk*

Keywords: ELECTROMECHANICAL OSCILLATIONS, FREQUENCY STABILITY, GRID-FOLLOWING FAST FREQUENCY RESPONSE, LOW INERTIA POWER SYSTEM, TRANSIENT STABILITY

Abstract

This paper investigates the impact of fast frequency response (FFR) on the transient stability of power systems. Focus is paid on the effects of FFR injection location within the transmission network. To allow the analysis to be easily generalised to other low inertia systems, a test system incorporating wind generation and HVDC interconnectors has been used. The FFR is provided by distributed storage devices with grid-following converters. It is shown that FFR can reduce transient stability despite the fact that frequency excursions are arrested. Synchronous generators in the system that are initially operating with a high relative angle displacement and which have low synchronous kinetic energy are considered critical with respect to this analysis. FFR delivered electrically close to critical generators is shown to cause larger angle divergence and will result in a greater chance of transient instability. Variations in system inertia, FFR capacity, disturbance location and network topology have also been studied to establish how severely the transient stability is affected when FFR is delivered at different locations within the system.

1. Introduction

Power systems are going through a period of radical change as converter interfaced generation (CIG) sources proliferate. CIGs do not inherently contribute to synchronous kinetic energy (or *inertia*) as compared to conventional synchronous generators (SGs), posing challenges concerning the frequency stability of future power systems [1]. Maintaining frequency stability following large disturbances by relying only on the existing primary frequency control schemes of SGs will prove difficult as these schemes are not fast enough to arrest frequency excursions in low inertia systems [2]. This will also give rise to an increase in system operational costs and carbon emissions. Conversely, providing fast frequency response (FFR) from numerous distributed CIGs within power systems is widely recognised as a cost-effective way to alleviate the concern of deterioration in frequency stability. With supplementary frequency control applied, FFR can be delivered from various technologies, dependent on different operational characteristics [1], [2].

Selecting the suitable placement of FFR within power systems needs to be addressed in order to keep the system operational and stable. The majority of the work published has focused on frequency stability improvement (as expected), for example [3], [4]. Studies to date, however, have rarely considered the impact of FFR on transient stability. The large-scale penetration of CIGs not only leads to reduction of the whole system inertia, but also results in significant variations in regional inertia. Larger frequency deviations and angle divergence will be seen in areas with lower inertia when the system is subjected to a disturbance. Issues may arise when FFR services are provided at points in the system electrically distant from the disturbance as (1) it increases the angle separation with respect to neighbouring regions [5], and (2) it leads to a larger amount of power flowing through transmission lines, possibly triggering protection schemes, which could eventually cause system splitting [6].

The interaction between FFR and transient stability has recently attracted attention of the transmission system operators (TSOs) who control electricity transmission networks with low inertia and tight transmission constraints, such as Iceland [6] and the Great Britain (GB) [7]-[9]. In [7], FFR has been demonstrated to have undesirable effects on transient stability when local frequency measurement is used, though frequency stability is maintained. This is primarily due to the spurious operation of the FFR devices as a result of variations in regional inertia. In order to accurately capture the regional variations in frequency dynamics, FFR schemes based on Wide Area Measurement System (WAMS) have been developed [6]-[9]. In this way, FFR is allocated to counteract the power deficit within centres of inertia of the system therefore minimising the detrimental impact on transient stability.

Although WAMS-based FFR schemes have been shown to be effective at preventing transient instability, it has exclusively been used in Icelandic power system due to lack of synchrophasor measurements in operation as well as the complexities in implementing such a scheme. At present FFR is therefore still commonly applied by using local measurements, for example the Dynamic Containment (DC) service procured by U.K. National Grid Electricity System Operator (NGESO) [10]. In addition to this, the underlying physical mechanism of how FFR impacts transient stability is not well understood and requires thorough investigation.

This paper investigates the impact of FFR on transient stability considering varying injection locations. The mechanism of how FFR affects the electromechanical oscillations of the SGs is explained through the use of a mixed AC/DC power system. Distributed battery storage devices with grid-following

converters are used to provide FFR. Deterioration in transient stability caused by FFR is highlighted by considering multiple factors, including system inertia, FFR capacity, disturbance location and network topology. The work presented in this paper is of significance as it allows the TSOs to be more confident when procuring FFR services or designing new stability services. It should be noted that the use of the acronym FFR within this document is generic and differs from the NGESO term Firm Frequency Response.

2. Modelling and Analysis

2.1. Test system description

A 29-node, 6-zone network is used as the test system throughout this study, shown in Fig. 1. This represents a reduced order equivalent model of the possible future GB transmission system. The representative GB network was first introduced in [11] and further developed in [12] for small-signal stability studies. Each node in the network represents an area containing large amounts of generation and/or demand in the GB system. The system is split into 6 zones based on the regional split of the network as given in [13] but with the B4 boundary separating the Scottish network into Zone 1 and Zone 2.

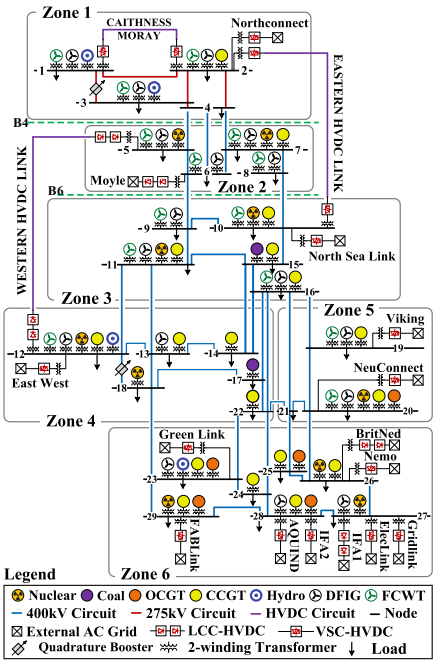

Fig. 1 GB 29-node, 6-zone test system diagram.

All SGs are represented by full six-order models with the dynamic parameters selected from [14] to represent distinct generating units. Coal-fired, gas-fired, and hydro units use the IEEE-DC1A exciter whilst nuclear units are equipped with the IEEE-ST1A exciter. All SGs also operate with governor systems with a dead band of ±15 mHz: coal-fired and nuclear units with the WSIEG1 governor, gas-fired units with the GASTWD governor and, hydro units with HYGOV governor. Both the hydro units at Node 1 and Node 3 are equipped with finely tuned IEEE-PSS1A power system stabilisers (PSSs) such that operating conditions that are stable with respect to small-signal stability are established. System loads use a ZIP model wherein the coefficients are selected based on [15]. Generic models for representing wind generation, including DFIG and FCWT [16], are used in this study. Both LCC-HVDC and VSC-HVDC systems are modelled as dynamic average-value models with *P-Q* control [17]. Static Var Compensators (SVCs) are modelled with constant voltage control to improve local voltage stability. Power system modelling is performed using DIgSILENT PowerFactory 2019.

The system generation and demand are determined using forecasted data from NGESO for the year 2030. The installed capacity for each type of generation is obtained from [18]. Two loading conditions of the Two Degrees Scenario given in [19] are used to alter the system inertia level: Winter Peak demand of 62 GW and Summer P.M. demand of 35 GW. With these loading conditions, the GB system operates with high power flows from northern generation zones to southern demand centres. Transmission circuits and shunt reactive compensation parameters are obtained from [13]. For the purpose of modelling scenario creation, the stochastic power carried through the interconnectors to/from the synchronous grids of Ireland, Nordic and Continental Europe are considered independent of each other, as well as stochastic wind generation at different nodes in the test system. The proportion of active power dispatch of the interconnectors are set to be identical if they are connecting to the same synchronous grid of Europe. The CCGT at Node 16 is the reference machine for the rotor angle in the system. Further system details can be found in [12].

2.2. Large disturbance modelling

In this study, only under-frequency events are considered. This is modelled by creating a sudden load connection at the target bus. This disturbance load is considered voltage independent and active power only. The disturbance is always sized at 1320 MW, equivalent to the Normal Infeed Loss Risk for the GB system. Such a disturbance not only leads to reasonably large frequency deviations that may require support from FFR devices, but it also enables analysis of the interaction between FFR and transient stability without the system naturally losing synchronism (following the disturbance but with no FFR).

2.3. Fast frequency response modelling

The control scheme of FFR in this study is implemented as the NGESO Dynamic Containment (DC) service [10]. DC is a post-fault service which aims to contain the system frequency within statutory range of [49.5, 50.5] Hz. The response curve of DC is depicted in Fig. 2, where the knee point frequency of the large proportional delivery is ±0.2 Hz.

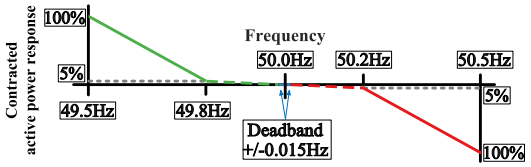

Fig. 2 Dynamic Containment – adopted from [10].

Despite the fact that various technologies may participate in the future FFR market, there is significant interest of using batteries to provide faster-acting frequency containment in the GB system due to their rapid controllability and great flexibility. A modified version of the generic model of battery energy

storage system (BESS) in PowerFactory [20] is used in this study as the DC provider accordingly. The frequency controller alongside the active power control loop is displayed in Fig. 3. The delay of DC output is implemented using standard time-delay function. A ramp limiter is added to the outer active power control loop in order to prevent the batteries delivering large fast injections of power as specified in [10]. The total requirements for DC Low Frequency (DCLF) in winter and summer are determined using the data for the year 2021, which are 800 MW and 1400 MW respectively.

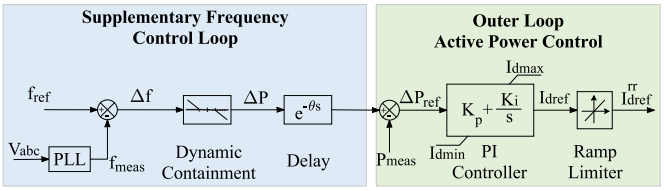

Fig. 3 Active power control loop of a BESS.

2.4. *Simulation analysis*

To reduce complexity of this initial investigation into the locational impact of FFR on transient stability, seven DC provision modes are considered. A base case with identical storage device installed at 29 nodes in the test system in order to provide the total DCLF during frequency excursions. These devices are all rated at 27.60 MW and 48.28 MW for the given winter and summer loading scenarios respectively. For the other six provision modes, it is assumed that the total DCLF is only provided in one zone and is evenly provided. This is justified by considering the availability of DC service provision is dependent on the day-ahead FFR market but not monopolised by particular providers. For example, in winter, if only the providers in Zone 1 are available for total DCLF provision, 4 identical storage devices are distributed at Node 1–Node 4 and all rated at 200 MW so that the total installed storage is 800 MW.

Dynamic transient simulations of 5 s long are performed for each of these DCLF provision modes with the disturbance occurs at t = 1 s (deviation from 50 Hz). To avoid possible detrimental impact of longer delays, the minimum initiation time of DLCF is selected for the simulations being performed – the delivery of active power begins 250 ms after the frequency deviation occurred [10]. The maximum rotor angle difference between the SGs ($\Delta\delta_{max}$) is used as transient stability index. $\Delta\delta_{max}$ values beyond 180° are considered unstable.

3. Results & Discussion

This section presents the analysis of the impact of variations in DCLF injection locations on transient stability. Three test cases described in Table 1 are used to highlight the key results as the system kinetic energy (∑SH) is reduced. To start with, Test case 1 is used to establish how transient stability is affected when the system operates with high levels of kinetic energy (DCLF requirements are small accordingly). Test case 2 is used to elaborate how the FFR-induced impacts change with reduced system inertia as well as increased DCLF requirements. Finally, Test case 3 is used to represent a typical operating condition in summer in order to ascertain if improper DCLF injection locations may degrade transient stability. The system non-synchronous penetration (SNSP) level is used as an indicator to represent the ratio of the total power generated by wind and imported HVDC divided by the total system demands and HVDC interconnector exports [21].

Table 1 Test case parameters

Test case	Study period	DCLF (MW)	Demand (GW)	SNSP ratio (%)	∑SH (GVA·s)
1	Winter	800	62	31	243
2	Summer	1400	35	31	145
3	Summer	1400	35	54	101

3.1. *Test case 1: 243 GVA·s*

This case represents a heavily loaded scenario (62 GW) where the system is initially operating with 31% penetration of non-synchronous generation. Fig. 4 presents the effects of DCLF delivered in different zones where the disturbance is at Node 6.

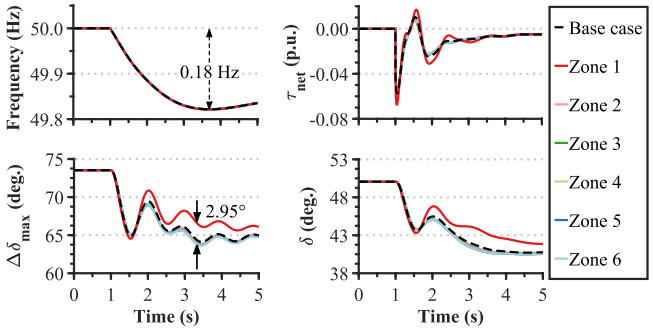

Fig. 4 For Test case 1: Responses of the system COI frequency, the maximum rotor angle difference of the SGs ($\Delta\delta_{max}$), CG's net torque (τ_{net}), and CG's angle with respect to the rotor angle of the reference machine (δ) following the disturbance (N.B. some lines are coincident as the numerical results achieved are only slightly changed with varying the injection location of DCLF).

In terms of the system frequency stability, the provision of DCLF in different zones is equivalent as identical frequency nadir has been observed, which is 49.82 Hz. Whereas for the transient stability, the locational impact of DCLF in Zone 1 can be clearly distinguished from that of other zones. Looking at the trajectories of the system's $\Delta\delta_{\max}$, greater values of $\Delta\delta_{max}$ can be seen following the initial swing after the disturbance when delivering the DCLF service in Zone 1. The largest difference between the resultant $\Delta\delta_{\max}$ values is 2.95°.

The reason why the same frequency nadir is maintained can be explained by considering the conservation of energy in the system. During the first few seconds after the disturbance occurs, as long as the same amount of energy is injected from the storage devices into the system, the initial power deficit in the system will be identically counteracted no matter where the injections occur. Note that the centre of inertia (COI) frequency is used for comparison here so that local effects are neglected.

Both the steady state (initial) rotor angle displacement and the inherent synchronous kinetic energy of the SGs are of primary significance with respect to the analysis of transient stability within this study. In particular the SG that is initially operating

with a large power angle and a low synchronous kinetic energy can be considered critical. This is because the physical impact of the arresting power injections on the system could be increased by their injection location with respect to this generator. These aspects will be further elaborated in the remainder of this section. By the resulting mechanism, the CCGT generator at Node 2 is considered as the critical generator (CG) in this system. Not only does it always experience the greatest positive steady state rotor angle displacement with respect to the reference machine, but it also has a relatively low synchronous kinetic energy in this system (throughout the three test cases presented, its kinetic energy is 7.46%, 16.78% and 16.11% of the SG with the largest kinetic energy respectively).

The locational impact of DCLF on the CG is presented by viewing the torque imbalance and the change in angular position of its rotor relative to the reference machine as displayed in Fig. 4. Starting with the well-known swing equation, following a power imbalance around the network, due to mechanical constraints, the mechanical power within the generator cannot change instantly. Thus the input mechanical torque placed on the rotor remains approximately constant during the timescales of interest. Whereas the propagation of electrical power through the system is comparatively quickly and in large quantities. The torque imbalance can thus be considered to be predominantly determined by the change in the output electrical torque. Looking back to the diagram of the GB network in Fig. 1, compared with the possible injection locations in Zone 2 to Zone 6, the locations in Zone 1 are adjacent to the CG at Node 2. Delivering the rebalancing service in Zone 1 is therefore far more likely to lead to greater change in the output electrical torque of the CG – resulting in larger torque imbalance (τ_{net}) placed on its rotor as shown in Fig. 4.

As previously discussed, the CG has a comparatively small amount of synchronous kinetic energy in this network, causing its rotor speed to change faster than other machines following the initial disturbance and the subsequent power injections. The system experiences large angle swings if the CG and the slower machines are not accelerating (or decelerating) together. When delivering the DCLF service in Zone 1 in particular, greater speed difference would be seen as well as the system angle separation. Furthermore, considering the CG is initially operating with the greatest power angle in the system, the change in the system's $\Delta\delta_{\text{max}}$ would be heavily dominated by the change in the angular position of the CG. That is why the provision of DCLF in Zone 1 has the greatest impact on the transient stability of the system.

It should be also noted that the frequency drop in this case is merely 0.18 Hz which does not reach the knee point frequency of the large delivery of the DCLF service (– 0.2 Hz). As such, only a small quantity of power has been injected into the network with a comparatively low ramp-up rate following the disturbance and hence, the overall physical impact imposed on the CG is relatively small.

3.2. Test case 2: 145 GVA·s

In this case, the system inertia is reduced by 40% from Test case 1. This case represents a light loading scenario (35 GW) but with the same penetration level of non-synchronous generation as Test case 1 (31%). The disturbance location and size remain unchanged but the requirement for the DCLF service is increased from 800 MW to 1400 MW as the available synchronous inertial response reduces with the system demand. Fig. 5 shows the corresponding transient responses for this case. Note that the power output from the BESS in different zones has been normalised for comparison.

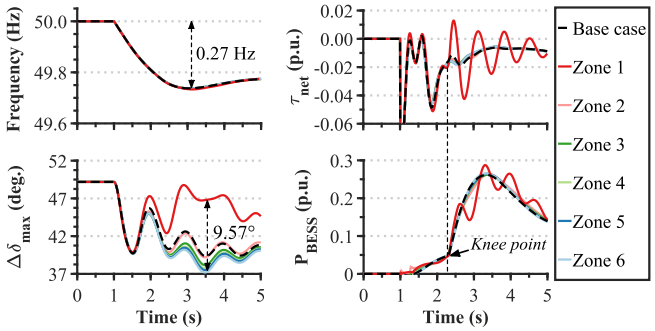

Fig. 5 For Test case 2: Responses of the system COI frequency, the maximum rotor angle difference of the SGs ($\Delta\delta_{max}$), CG's net torque (τ_{net}), and typical power output from the BESS (P_{BESS}) following the disturbance.

As with Test case 1, the provision of the DCLF service in different zones has the same effect on the system frequency stability, though a greater frequency drop (0.27 Hz) is observed. However, the rotor swings are shown to be much larger and faster with the system inertia reduced, resulting in noticeable disparity between the DCLF locational impact on the transient stability. The largest difference between the resultant values of $\Delta\delta_{\text{max}}$ is increased to 9.57° (compared to 2.95° previously). The impact is most pronounced when delivering the DCLF service in Zone 1 (as before). Providing the DCLF in Zone 6 is shown to be advantageous and improve both frequency stability and transient stability following the disturbance.

The large variation in $\Delta\delta_{\text{max}}$ caused by the power injections in Zone 1 can be explained by looking at the power output from the BESS incorporation with the torque imbalance of the CG as displayed in Fig. 5. After the disturbance, with a delay of 250 ms, the batteries start to deliver the balancing service but with a small delivery characteristic. This explains the very little disparity between the impact of DCLF injection location on the CG following the initial swings after the disturbance. Once the frequency drops below 49.8 Hz, larger and faster injections of power are delivered from the batteries according to the DCLF control strategy (see Fig. 2). With large quantities of power delivered, it is likely that the CG would experience greater change in torque imbalance (τ_{net}), particularly when the injections are being located in Zone 1. It can clearly be seen that the injections in Zone 1 are robust to switch the CG's negative torque (– 0.02 p.u.) to positive (0.017 p.u.), further accelerating the rotor accordingly. As a result, the angular difference between the CG with respect to the slower machines is advance, leading to large excursions of $\Delta\delta_{\text{max}}$.

It is also evident from Fig. 5 that the batteries' power output in Zone 1 contains oscillations compared to that of other zones. This disparity is due to the fact that local frequency at the target

node is used to provide the DCLF service and, the frequency nadir and ROCOF are not uniform around the system (comparing to the COI frequency). In particular an area, such as Zone 1 in this system, with sparse distribution of inertia can experience large and fast frequency variations after a disturbance. Providing the locational balancing service in such an area would risk the transient stability of the system and should, therefore be avoided through appropriate service procurement.

With the electrical distance between the DCLF injection location and the CG increased (from Zone 2 to Zone 6 in this system), the additional power from the batteries is mainly absorbed by other machines and hence the impact on the CG is gradually diminished. The CG is therefore not be further accelerated, leading to similar variations in $\Delta\delta_{\max}$.

3.3. Test case 3: 101 GVA·s

In this case, the system inertia has been further reduced (by 60% from Test case 1). The system is operating with the SNSP ratio of 54%, possibly representing a typical condition in the future operation of the GB system. As with Test case 2, the disturbance size, disturbance location and, DCLF requirements remain unchanged. Transient responses after being subjected to the disturbance at Node 6 are displayed in Fig. 6. Due to space limitations, particular focus will be paid to the impact of DCLF provision in Zone 1 on the transient stability though all possible DCLF provision modes are simulated to generate the full set of results.

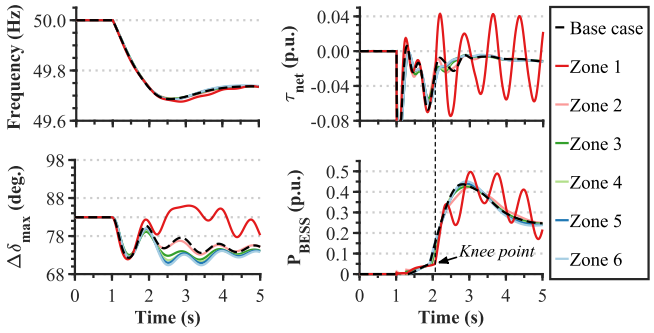

Fig. 6 For Test case 3: Responses of the system COI frequency, the maximum rotor angle difference of the SGs ($\Delta\delta_{max}$), CG's net torque (τ_{net}), and power output from the BESS (P_{BESS}) following the disturbance.

Unlike the previous cases presented in this study, the power injections in Zone 1 in this case lead to greater values of $\Delta\delta_{max}$ which easily exceed the initial value of 83.11°. The further reduction in system inertia also highlights the likelihood that the CG will be subjected to persistent oscillations due to the activation of the large proportional delivery of the DCLF service in Zone 1. This can be explained by the fact that the power output from the BESS in Zone 1 is always in phase with the electromechanical oscillation of the CG. Similar conditions in other systems (i.e., FFR injections that are in phase with the electromechanical oscillations of the nearby SGs) would likely result in similar criticality.

This may not prove to be problematic, but this detrimental impact could become worse when the system is further stressed. To highlight the key problem, two further cases are used where the system is still operating with the same generation and loading as Test case 3: an *alert case* represents the disturbance location moved to load centres, and an *extreme case* represents a high impedance network topology.

For the *alert case*, the frequency disturbance is moved to Node 28 and all transmission lines are in service. Fig. 7 displays the transient responses for this case.

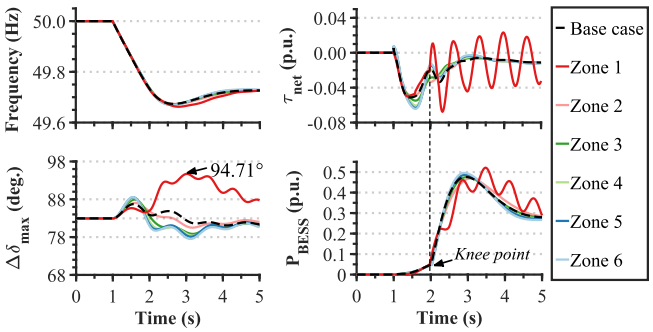

Fig. 7 For the *alert case*: Responses of the system COI frequency, the maximum rotor angle difference of the system ($\Delta\delta_{max}$), CG's net torque (τ_{net}), and power output from the BESS (P_{BESS}) following the disturbance at Node 28.

Unlike the cases when the disturbance is at Node 6, the trajectories of $\Delta\delta_{\max}$ rise up instantly when the system is subjected to the disturbance at Node 28. This inherently makes the system prone to transient instability issues and particularly, the arresting power injections in Zone 1 have once increased the value of $\Delta\delta_{\max}$ to 94.71°, which is 11.60° greater than the initial value (83.11°).

For the *extreme case*, the system is operating with a key AC tie-line removed from service – the 400 kV double-circuit transmission line 6-9 (crosses the boundary B6). This line is considered critical as it provides one of the main paths for power flow from Scotland to England. This has therefore increased the equivalent impedance between the Scottish and English networks. As a result, the system is initially operating with a greater angle separation of 112.46°. The size of the frequency disturbance remains unchanged; the disturbance is located at Node 6 in order to isolate the inherent detrimental impact of the disturbance at Node 28 on the transient stability. To illustrate the findings clearly, transient studies have been performed for two possible injection zones: Zone 1 and Zone 2, as displayed in Fig. 8.

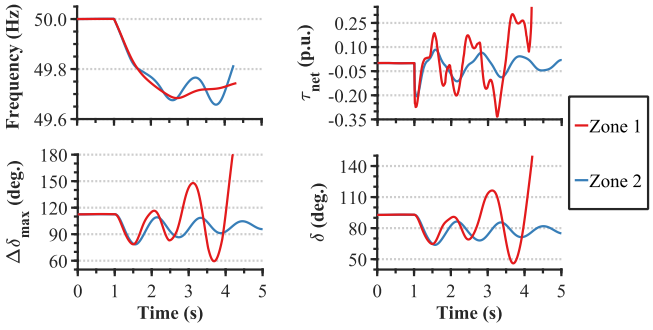

Fig. 8 For the *extreme case*: Responses of the system COI frequency, the maximum rotor angle difference of the SGs ($\Delta\delta_{max}$), CG's net torque (τ_{net}), and CG's rotor angle with

respect to the rotor angle of the reference machine (δ) following the disturbance.

Loss of synchronism occurs between the critical generator and the rest of the system when delivering the DCLF in Zone 1, wherein increasing amplitude of rotor oscillations can clearly be seen. With the DCLF provision moved to Zone 2, a transition from an unstable to stable system operation is achieved.

4. Conclusions

This study highlights the unexpected impacts that an FFR scheme may have on transient rotor angle stability, as well as the inherent links between frequency and transient stability which are not often considered concurrently. FFR injection location has been critically investigated to establish the effects on system stability. This study has important implications for safely assigning FFR in future low inertia systems. It has revealed that FFR can have detrimental effects on transient stability, despite the fact that frequency excursions are arrested within statutory limits. It shows that transient stability is strongly affected by the FFR injection location with respect to the critical generator, which can be identified by considering generators with a combination of low synchronous kinetic energy and high steady state rotor angle displacement. Due to the additional torque imbalance imposed on the rotor, delivering large and fast power injections in the area where critical generators are located is shown to increase angle divergence and reduce transient stability. Conversely, rapid power injections electrically distant from the critical generator are shown to have a much less detrimental impact on transient stability.

Greater deterioration in transient stability caused by FFR, for example persistent electromechanical oscillations, has also been shown for situations when the system operates with lower levels of synchronous kinetic energy. This is particularly true when the disturbance occurs near demand centres or under the presence of high impedance and low connectivity (i.e., when generation zones are electrically distant from demand centres). These findings suggest the necessity of allocating FFR in areas with reasonable electrical distance from any critical generators. Caution must be applied when any inter-area AC tie-line is removed from service to ensure FFR is safely located.

It is easy to envisage that FFR injections are more likely to increase the risk of transient instability when implementing derivative controller or multi-step response (proportional to the power deficit), as such FFR schemes presently gain popularity in enhancing frequency stability in future low inertia systems with high divergence in regional inertia. Future work should investigate mitigation strategies to avoid detrimental impacts by incorporating various FFR schemes.

5. References

[1] F. Milano, F. Dorfler, et al.: 'Foundations and challenges of low-inertia systems (Invited Paper)', 20th Power Syst. Comput. Conf. Dublin, Ireland, June 2018, pp. 1–25

[2] H. Karbouj, Z. Hussain, et al.: 'Non-synchronous fast frequency reserves in renewable energy integrated power systems: A critical review', Int. J. Electr. Power Energy Syst., 2019, 106, (March), pp. 488–501

[3] B. K. Poolla, S. Member, D. Groß, et al.:'Placement and Implementation of Grid-Forming and Grid-Following Virtual Inertia and Fast Frequency Response', IEEE Trans. Power Syst., 2019, 34, (4), pp. 3035–3046

[4] D. Kez, et al.: 'A Comparative Assessment of Battery Energy Storage Locations in Power Systems with High Wind Power Penetrations', in 2020 EEEIC, pp. 1-6

[5] D. Wilson, J. Yu, N. Al-Ashwal, et al.: 'Measuring effective area inertia to determine fast-acting frequency response requirements', Int. J. Electr. Power Energy Syst., 2019, 113, (February), pp. 1–8

[6] D. Wilson, et al.: 'Iceland Operational Experience of Synchrophsaor-based Fast Frequency Response and Islanding Defence', Cigre Paris Session, Aug 2018

[7] D. Wilson, S. Clark, S, Norris, et al.: 'Advances in Wide Area Monitoring and Control to address Emerging Requirements related to Inertia, Stability and Power Transfer in the GB Power System', Cigre Paris Session, 2016

[8] National Grid ESO, 'The Enhanced Frequency Control Capability (EFCC) project closing down report', April 2019, pp. 1–134

[9] Q. Hong, M. Karimi, M. Sun, et al.: 'Design and Validation of a Wide Area Monitoring and Control System for Fast Frequency Response', IEEE Trans, Smart Grid., 2020, 11, (4), pp. 3394–3404

[10] 'Dynamic Containment', https://www.nationalgrideso.com/industry-information/balancing-services/frequency-response-services/dynamic-containment

[11] K. R. W. Bell and A. N. D. Tleis, 'Test system requirements for modelling future power systems', in Power and Energy Society General Meeting, 2010, pp. 1-8.

[12] S. Asvapoositkul and R. Preece, 'Analysis of the variables influencing inter-area oscillations in the future Great Britain power system', 15th IET International Conference on AC and DC Power Transmission, 2019, pp. 1–7.

[13] 'Electricity Ten Year Statement (ETYS) 2020', https://www.nationalgrideso.com/research-publications/etys-2020

[14] P. M. Anderson and A. A. Fouad: 'Power system control and stability' (Wiley India Pvt. Limited, 2008, 2nd edn.)

[15] A.Perez Tellez: 'Modelling Aggregate Loads in Power Systems', MSc thesis, KTH Royal Institute of Technology, 2017

[16] P. Pourbeik et al.: 'Generic stability models for type 3 & 4 wind turbine generators for WECC', in 2013 IEEE Power & Energy Society General Meeting, 2013, pp. 1–5

[17] CIGRE Working Group, 'Guide for the development of models for HVDC converters in a HVDC grid', 2014.

[18] 'Electricity Ten Year Statement (ETYS) 2018', https://www.nationalgrideso.com/electricity-ten-year-statement-etys-archive

[19] 'Future Energy Scenario 2018', https://www.nationalgrideso.com/future-energy/future-energy-scenarios/fes-documents-archive

[20] DIgSILENT PowerFactory, 'Application Example, Battery Energy Storing Systems', 2010, pp. 1–28

[21] J. O'Sullivan, A. Rogers, et al.: 'Studying the Maximum Instantaneous Non-Synchronous Generation in an Island System—Frequency Stability Challenges in Ireland', IEEE Trans. Power Syst., 2014, 29, (6), pp. 2943–2951